25p

NASA TN D-1679

N63-13102
Code 1

TECHNICAL NOTE

D-1679

ON THE ANOMALOUS COMPONENT OF LOW-ENERGY GEOMAGNETICALLY TRAPPED PROTONS

A. M. Lenchek

Goddard Space Flight Center
Greenbelt, Maryland

NATIONAL AERONAUTICS AND SPACE ADMINISTRATION
WASHINGTON
February 1963

Copy 1

Code 1

ON THE ANOMALOUS COMPONENT OF LOW-ENERGY GEOMAGNETICALLY TRAPPED PROTONS

by

A. M. Lenchek
Goddard Space Flight Center

SUMMARY

The energy spectrum of trapped protons shows a pronounced variation with latitude at energies below 30 Mev. An anomalous, low-energy component is found on relatively high magnetic shells in the inner zone. The interpretation of this anomalous component in terms of the decay of albedo neutrons generated in the polar caps by solar cosmic rays is examined. This interpretation requires that the inner shells, where a normal spectrum is seen, should be shielded from the polar source. The intensity of albedo neutrons as a function of energy, latitude, and zenith angle is computed. The injection rate into specific trapped orbits is then evaluated and it is shown that those orbits where no anomalous component exists cannot be populated by the solar cosmic ray mechanism while the orbits where the anomalous component is seen can be populated. When the assumption is made that there is adiabatic trapping in this low energy region, lifetimes are long compared to the average interval between large injection events. Therefore, the anomalous component may represent an equilibrium phenomenon rather than a transient. This component should extend into the outer belt.

CONTENTS

LIST OF SYMBOLS

E	The energy of the secondary neutron and trapped proton.
$E_{max}(L)$	The maximum energy of a proton which remains trapped in the quiescent geomagnetic field.
$F(\omega)$	The equilibrium energy spectrum of differential intensity, given by Equation 40 (dimensionless).
$I(\lambda', x)$	The omnidirectional integral flux of primaries (at latitude λ') which have energies above 10 Mev at depth x.
$I_o(\lambda')$	The integral over the upper hemisphere of the integral unidirectional intensity of primaries above 10 Mev.
$\bar{J}$	The integral unidirectional intensity of solar cosmic rays averaged over a solar cycle.
J_o	The integral unidirectional intensity of solar cosmic rays above 10 Mev, evaluated at a latitude at which the cutoff energy is less than 10 Mev.
$J(E)$	The integral unidirectional intensity of trapped protons with energies above E.
$J(>R, y)$	The directional integral intensity of protons with residual range greater than R.
$j(E, L, \alpha_o)$	The differential unidirectional intensity of trapped protons.
$j_n(E, \lambda', \phi)$	The differential unidirectional intensity of albedo neutrons.
$j_n^*(E)$	The vertical intensity of neutrons at the pole.
L	Magnetic shell parameter, equivalent to r_o/r_e in a dipole field.
L_{min}	The minimum shell accessible to protons injected by polar cap neutrons.
ℓ	The attenuation length of neutrons passing through air.
$\mathfrak{M}$	The average mass per atom of the atmosphere.
$N(T)$	The probable number of neutrons emitted following an interaction with a proton energy T.
p_n/p_d	The neutron emission probability relative to deutron emission probability.
p_n/p_p	The neutron emission probability relative to proton emission probability.

p_n/p_a	The neutron emission probability relative to alpha particle emission probability.
$Q(E, \lambda', x)$	The production rate of neutrons of energy E at latitude λ' and depth x.
$q(E, L, \alpha_e; \lambda, \theta)$	The local injection rate giving number of protons injected/Mev-cm^3-ster-sec.
$\bar{q}(E, L, \alpha_o)$	The injection rate averaged over the spiral path.
$q(\lambda)$	The injection rate at λ averaged over one gyroperiod.
R	The range of solar proton in air.
R_o	$R(T_o)$.
R_1	$R(T_1)$.
$\bar{R}$	The mean range of the solar cosmic rays in model 1.
r	Geocentric distance.
r_e	The earth's equatorial radius.
r_o	The geocentric distance of a line of force measured in the equatorial plane.
S(E)	Evaporation spectrum.
$s(\alpha_o)\, r_o$	The length of the spiral path of a trapped particle, measured from the equatorial plane to a mirror point.
T	The energy of a solar proton.
T_o	The threshold energy of N^{14} (p, n) O^{14} reaction.
T_1	The cutoff energy of solar cosmic rays assumed in model 2.
$T_{1/e}$	The 1/e lifetime, the time over which the energy decreases to 1/e times the initial value.
t_o	The duration of solar cosmic ray event.
t_n	The mean lifetime of the neutron.
u	$\frac{R_o}{\ell \cos \phi}$.
v	Neutron velocity.
x	Atmospheric depth.
$y = x \sec \phi$	The slant depth of a point in the atmosphere.

α The local pitch angle, the angle between the velocity vector and the magnetic field.

α_o The equatorial pitch angle.

α-cone The cone swept out on the globe by the gyration of the velocity vector.

δ-cone A cone, of semiangle δ, drawn from a point in space to the earth; the cone is tangent to the earth's surface.

ϵ_3 The injection coefficient for orbits mirroring at NERV point number 3.

ϵ_4 The injection coefficient for orbits mirroring at NERV point number 4.

ϵ_{55} The injection coefficient under the assumption that the solar cosmic rays reach a latitude of 55 degrees and higher.

ϵ_{60} The injection coefficient under the assumption that the solar cosmic rays reach a latitude of 60 degrees and higher.

$\epsilon(L, \alpha_o)$ The injection coefficient, giving the rate of injection into an orbit in terms of the rate j_n^*/t_{nv}, corresponding to the decay rate of the vertical albedo intensity at the pole.

Θ Nuclear temperature.

Θ' The temperature appropriate to each stage of evaporation cascade.

θ The phase angle between the velocity vector and the meridian plane.

λ Magnetic latitude.

λ_c The latitude of the boundary of the polar cap.

λ_m Mirror point latitude.

λ' The geomagnetic latitude of a point on globe from which an albedo neutron is emitted.

$\lambda^\dagger$ The highest latitude on earth's surface attained by the α-trace.

$\overline{\rho}$ The density of atoms-and-ions/cm^3 averaged over a trapped orbit.

$\overline{\rho}_3$ The average density for orbits mirroring at NERV point number 3.

$\overline{\rho}_4$ The average density for orbits mirroring at NERV point number 4.

σ_o $\sigma(T)$ for $T > 10$ Mev.

σ_t The total cross section for neutron interaction in air.

$\sigma(T)$ The cross section for production of one neutron.

$\sigma_c(T)$ The cross section for compound nucleus formation as a function of proton energy.

$\Phi(\lambda', \phi)$ Defined by Equation 5.

$\Phi_1(\lambda' \phi)$ $\Phi(\lambda', \phi)$ for model 1.

$\Phi_2(\lambda' \phi)$ $\Phi(\lambda', \phi)$ for model 2.

$\Phi_3(\lambda' \phi)$ $\Phi(\lambda', \phi)$ for model 3.

Φ^* $\Phi(\lambda' > \lambda_c, \phi = 0)$.

ϕ The zenith angle of an albedo neutron upon leaving the atmosphere.

$\psi(x, \phi)$ The albedo angular distribution function, the ratio of albedo intensity at zenith angle ϕ to the vertical intensity at the pole.

$\Omega(L, a_o, \lambda)$ Defined by Equation 19.

ON THE ANOMALOUS COMPONENT OF LOW-ENERGY GEOMAGNETICALLY TRAPPED PROTONS

by

A. M. Lenchek
Goddard Space Flight Center

INTRODUCTION

Observations of geomagnetically trapped protons have recently been extended to energies as low as 8 Mev (Reference 1) by use of the Nuclear Emulsion Recovery Vehicle (NERV). The energy spectrum shows a pronounced variation with position in space. The spectrum on magnetic shells crossing the geomagnetic equator at geocentric distances r_o of approximately 1.5 earth radii r_e agrees well with theoretical predictions (References 2 and 3) based on injection by neutron albedo from galactic cosmic radiation (References 4 and 5).

However, the spectrum observed on shells at $r_o > 1.7\ r_e$ is anomalous in the sense that it is much steeper and more intense than the spectrum which results from "galactic" albedo, see Figure 1. It has been suggested (References 1 and 6) that the neutron albedo generated in the polar caps by the arrival of low-energy solar cosmic rays may result in trapped protons. Some discussions of the characteristics of the protons resulting from this effect have already been given (References 3 and 7). The object of this paper is to treat this mechanism more quantitatively than References 3 and 7 in an attempt to show that it can account for the NERV observations.

Three prominent features distinguish the solar cosmic rays from the galactic cosmic rays: (1) Solar cosmic rays arrive in intense bursts of short duration, the intensity typically decaying to normal in about a day, (2) arrive mostly at high latitudes, and (3) have a mean energy two or three orders of magnitude below that of the galactic radiation. Because of this last feature we may expect the number and energy spectrum of secondary neutrons to differ markedly from those produced by galactic cosmic rays: First, the high-energy spallation component should be almost totally absent. Second, the evaporation component should show a relatively lower temperature. Third, unlike the products of the global (i.e., galactic) radiation, most of the "polar" neutrons will be generated close to the top of the atmosphere (the range of a typical solar proton, with energy $T \lesssim 100$ Mev, is much shorter than the mean free path of the neutrons which have energies around 10 Mev).

Previous work on the albedo neutron energy spectrum (References 3, 4, 8, 9, 10, and 11) has been based on data referring to high-energy interactions involving primaries with energies in the Bev range. However, the primaries involved in the present paper have energies on the order of 10-100

Mev. We therefore must re-examine the neutron production process, concentrating on the reaction $N^{14}(p,n)O^{14}$.

In order to determine the spatial distribution of the trapped protons produced by this mechanism it is necessary to examine in detail the efficiency of trapping as a function of r_o and pitch angle. This, in turn, requires a knowledge of the angular distribution of the albedo intensity.

We therefore begin by examining the production of neutrons in the atmosphere by low energy cosmic ray protons. We then calculate the albedo intensity as a function of energy and zenith angle. Next we examine the injection coefficient as a function of energy, altitude, and pitch angle. It is found that the results of these calculations depend quite strongly on the form of the primary energy spectrum. However, the spectrum of the solar beam is variable from one event to another. We therefore carry out the calculations for several different spectra.

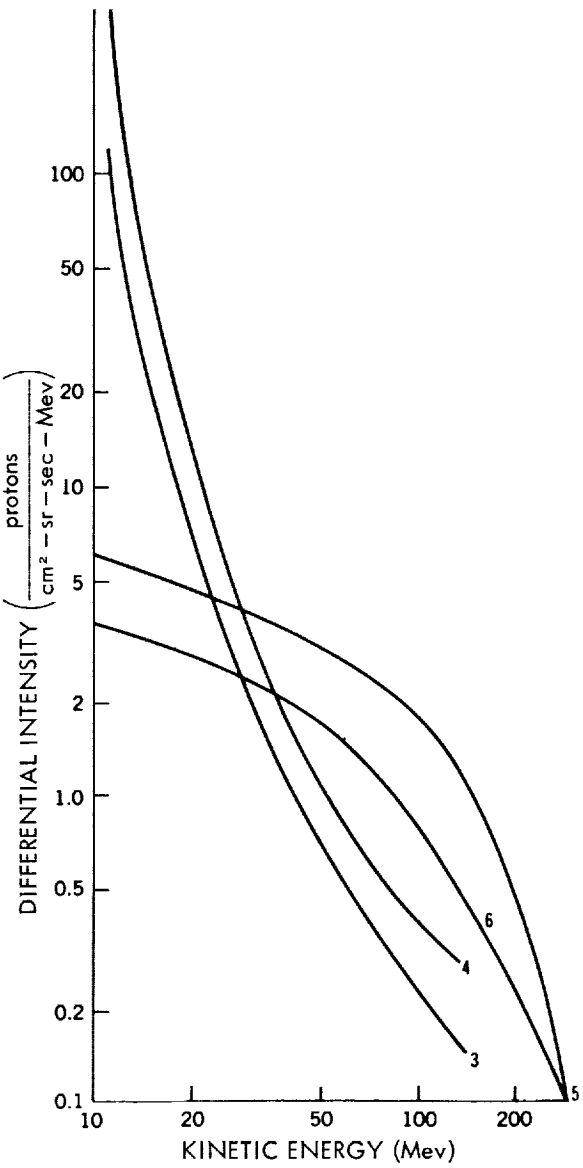

Figure 1 - Energy spectra of trapped protons on four different magnetic shells measured by the Nuclear Emulsion Recovery Vehicle program on September 19, 1960. Figure courtesy of Naugle and Kniffen. Altitudes and shell parameters L of the points are: point 3, alt. 1600 km, L = 1.79; point 4, alt. = 1884 km, L = 1.72; point 5, alt. 1600 km, L = 1.54; and point 6, alt. 1400 km, L = 1.47.

PRODUCTION OF NEUTRONS

When protons with energies $T \lesssim 100$ Mev strike the atmosphere, the major source of secondary neutrons is the interaction of protons with N^{14}. Experimental data on the cross section for neutron production in this interaction is scanty. The neutron yield when 32 Mev protons bombard a thick nitrogen target is known (Reference 12). The yield, 3.2×10^{-3} neutrons per proton, is comparable to the yield from oxygen. The energy spectrum of the neutrons produced in thin target experiments on nitrogen at 17.3 Mev (Reference 13) and at 31.5 Mev (Reference 14) shows several poorly resolved groups which tend to merge into a continuum at low energy. It is possible to represent the spectrum approximately in the form of an evaporation spectrum with a "temperature" around 4 Mev.

In this energy range, the mean free path of a nucleon is short compared to the nuclear diameter, suggesting that spallation may be less favored than compound nucleus formation. This observation,

plus the evaporation-like nature of the neutron spectra, lead us to investigate the cross section for neutron production on the basis of evaporation theory. However, we rely on evaporation theory only to reveal the energy dependence and we use the observation of Tai et al. (Reference 12) for normalization.

Thus, we set $\sigma(T) = \sigma_c(T)\ N(T)$, where $\sigma_c(T)$ is the cross section for compound nucleus formation and $N(T)$ is the probable number of neutrons emitted. We compute $\sigma_c(T)$ in the semiclassical approximation (Reference 15), which is valid for T greater than about twice the Coulomb barrier, that is, for $T > 6$ Mev. We evaluate $N(T)$, using the theoretical results of LeCouteur (Reference 16), by computing the relative probabilities P_n/P_p, P_n/P_α and P_n/P_d for emission of a neutron or proton; neutron or alpha particle; and neutron or deuteron. Multiple particle emission is considered up to three-particle cascades although, since all the required separation energies are not available, triple cascades can only be estimated. In computing cascades it is assumed that all particles except the last are emitted with the average energy of those emitted in each stage. The relation between the nuclear temperature Θ and the excitation energy is assumed to be given by the usual degenerate Fermi-gas model of the excited nucleus.

It is found that proton emission is most likely in the first stage of de-excitation. The calculated $\sigma(T)$ rises rapidly as T is increased above the threshold $T_o = 6.4$ Mev, and then levels off at about 10 Mev, attaining a maximum value of only about 70 mb. Multiple emissions tend to increase this figure at higher energies. The data of Tai et al. can be fitted by assuming that $\sigma(T) = 0$ for $T < 10$ Mev and $\sigma(T) = \sigma_o = 80$ mb for $T > 10$ Mev. We shall therefore adopt this simple model for $\sigma(T)$.

We assume the evaporation spectrum is given by

$$S(E) = E\Theta^{-2}\, e^{-E/\Theta} \text{ neutrons/Mev} \tag{1}$$

per interaction, where E is the neutron energy. In cascades in which more than one neutron is emitted, Θ is an average value found by assuming that all particles except the last are emitted with $E = 2\Theta'$ (Θ' is the temperature appropriate to each state), weighting the several Θ' values by the fraction of the neutrons belonging to each stage, and summing over stages. It is then found that Θ is a quite slowly varying function of T, varying only between 3 and 5 Mev as T varies from threshold to 50 Mev. We may therefore take $\Theta = 4$ Mev as an average, independent of T. This is an important simplification since it implies that the neutrons are generated with the same spectrum at all atmospheric depths.

We therefore conclude that (1) the neutron production is adequately represented (approximately) by a constant cross section of 80 mb with an effective threshold of 10 Mev, (2) the energy spectrum of the neutrons is Maxwellian with temperature 4 Mev, and (3) the production angular distribution is isotropic.

ALBEDO INTENSITY

We turn now to the question of the differential unidirectional intensity of neutrons leaving the atmosphere. We must compute the production rate as a function of atmospheric depth and, assuming

for simplicity an exponential attenuation of the emerging beam, compute the escaping intensity as a function of energy and zenith angle.

The production rate at atmospheric depth x and at geomagnetic latitude λ' is

$$Q(E,\lambda',x) = \frac{\sigma_o I(\lambda',x)\ S(E)}{\mathfrak{M}} \quad \frac{\text{neutrons}}{\text{Mev-gm-sec}}, \tag{2}$$

where $\mathfrak{M}$ is the average mass per atom of the atmosphere and $I(\lambda',x)$ is the omnidirectional integral flux of primaries which have energies above 10 Mev at depth x.

The differential unidirectional intensity of albedo neutrons leaving the atmosphere at the zenith angle ϕ is obtained by integrating $Q(E,\lambda',x)$ over a slant path, assuming a plane stratified atmosphere:

$$j_n(E,\lambda',\phi) = \frac{1}{4\pi \cos\phi} \int_o^\infty Q(E,\lambda',x)\ \exp\left[\frac{-x}{\ell \cos\phi}\right] dx \quad \frac{\text{neutrons}}{\text{Mev-cm}^2\text{-ster-sec}}. \tag{3}$$

Here ℓ is the attenuation length, which we approximate by $\mathfrak{M}/\sigma_t$ where σ_t is the total cross section in air (Reference 17). In the energy range in which we are interested (about 5-30 Mev), we can assume $\ell = 15$ gm/cm^2, independent of energy. Then

$$j_n(E,\lambda',\phi) = \frac{\sigma_o \ell}{4\pi \mathfrak{M}}\ I_o(\lambda')\ S(E)\ \Phi(\lambda',\phi), \tag{4}$$

where

$$\Phi(\lambda',\phi) = \frac{1}{\ell \cos\phi} \int_o^\infty \left[\frac{I(\lambda',x)}{I_o(\lambda')}\right]\ \exp\left(\frac{-x}{\ell \cos\phi}\right) dx. \tag{5}$$

Here $I_o(\lambda')$ is the integral over the upper hemisphere of the integral directional intensity of primaries above 10 Mev.

Let $j_n^*(E)$ denote the vertical intensity of neutrons at the pole. The boundary of the polar cap is at latitude λ_c, the latitude at which the geomagnetic cutoff is 10 Mev. We shall express $j_n(E,\lambda',\phi)$ in terms of $j_n^*(E)$ as

$$j_n(E,\lambda',\phi) = j_n^*(E)\ \Psi(\lambda',\phi). \tag{6}$$

Thus,

$$\Psi(\lambda',\phi) = \frac{\Phi(\lambda',\phi)}{\Phi(\lambda' > \lambda_c,\ \phi = 0)}.$$

We shall denote $\Phi(\lambda' > \lambda_c,\ \phi = 0)$ by Φ^*. Then

$$j_n^*(E) = \frac{\sigma_o J_o \ell S(E) \Phi^*}{2\pi} , \tag{7}$$

where J_o is the integral directional intensity (in particles/cm^2-ster-sec) of solar cosmic rays above 10 Mev, evaluated at a latitude where the cutoff energy is less than 10 Mev. We assume J_o is isotropic; hence $J_o = I_o/2\pi$. Before we can evaluate the albedo distribution function $\Psi(\lambda', \phi)$ we must discuss the spectrum of the solar beam, since this determines $I(\lambda', x)/I_o(\lambda')$ appearing in Equation 5.

THE SOLAR BEAM

Until recently no direct observations of the spectrum of solar cosmic rays were available. However, the spectra during the events of September 3, 1960, and November 12-15, 1960, were directly measured (References 18 and 19). In the September 3 event, a Geiger counter and nuclear emulsions carried on the same rocket yielded an integral proton spectrum that was almost flat up to about 100 Mev with an intensity $J_o \sim 19$ particles/cm-ster-sec above 22 Mev. In the November event the integral spectrum was close to $T^{-1.7}$ (from 10-100 Mev) with an intensity $J_o \gtrsim 2 \times 10^3$ particles/cm^2-ster-sec above 10 Mev. In both cases the intensity was isotropic over the upper hemisphere.

EVALUATION OF THE DISTRIBUTION FUNCTION

We shall consider three cases: (1) exponential variation of Q with depth, (2) primary spectrum flat up to 100 Mev, and (3) primary spectrum $J_o \propto T^{-1.7}$.

Model 1:

We assume

$$\frac{I(\lambda', x)}{I_o(\lambda')} = e^{-x/\bar{R}} , \tag{8}$$

where $\bar{R}$ is the mean range of the solar cosmic rays. Inserting into Equation 5, we obtain

$$\Phi_1(\lambda', \phi) = \frac{\bar{R}}{\ell}\left(\cos\phi + \frac{\bar{R}}{\ell}\right)^{-1} . \tag{9}$$

Taking $\bar{R}$ to be the range of a representative primary ($T < 100$ Mev), we find that $\bar{R}$ will be small compared with ℓ, giving an anisotropic albedo with a maximum at the horizontal.

Model 2:

Assume an isotropic intensity J_o = constant up to T_1 and $J_o = 0$ above T_1. Convert to a range spectrum and transform to a depth x by noting that at the slant depth $y = x \sec\phi$ the directional integral intensity $J(> R, y)$ of protons with residual range greater than R equals the primary intensity

$J_o(R+y)$ for $R+y < R(T_1)$ and is zero for $R+y > R(T_1)$. Denote $R(T_1)$ by R_1. Then integrate over the hemisphere to obtain

$$\frac{I(\lambda',x)}{I_o(\lambda')} = 1 - \frac{x}{R_1 - R_o} \quad \text{for} \quad x \leq R_1 - R_o = x_o \tag{10}$$

and

$$I(\lambda',x) = 0 \quad \text{for} \quad x > x_o .$$

Here $R_o = R(T_o) = 0.15$ gm/cm^2 and $R_1 = R(T_1) = 7.5$ gm/cm^2 assuming $T_1 = 100$ Mev.

Inserting Equation 10 into Equation 5, we easily find

$$\Phi_2(\lambda',\phi) = 1 - \frac{\ell \cos\phi}{x_o}\left(1 - e^{-\frac{x_o}{\ell \cos\phi}}\right). \tag{11}$$

Since $x_o \sim \ell/2$ we again find a moderate anisotropy with $\Phi_2(\lambda', \pi/2)/\Phi_2(\lambda',0) = 4.71$.

Model 3

Assume $J_o = AT^{-1.7}$. Using the familiar relation $R(T) = \text{constant} \times T^{1.7}$ we then find

$$\frac{I(\lambda',x)}{I_o(\lambda')} = 1 - \frac{x}{R_o} \ln \frac{R_o + x}{x} \tag{12}$$

and

$$\Phi_3(\lambda',\phi) = 1 + e^u Ei(-u)\left[\frac{1}{u} - 1\right] - \frac{1}{u}(\gamma + \ln u), \tag{13}$$

where $u = R_o/\ell \cos\phi$, $-Ei(-u)$ is the logarithmic integral and $\gamma = 0.577$ is Euler's constant. We find $\Phi_3(\lambda',0) = 0.025$ and $\Phi_3(\lambda', \pi/2) \approx 1$.

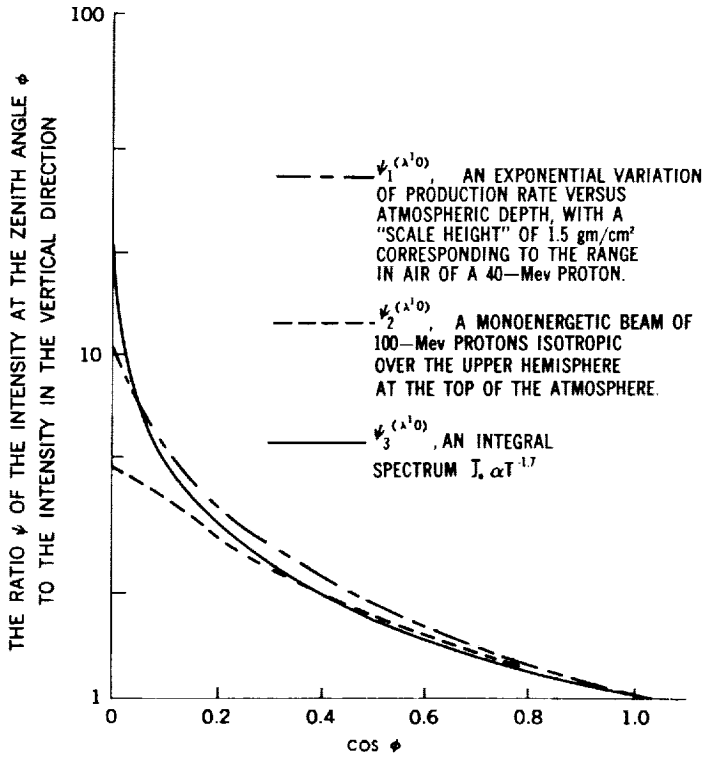

Figure 2 - Angular distribution functions of albedo neutrons generated by low-energy cosmic rays. In each case a constant cross section with threshold 10 Mev is used. Exponential attenuation of the emerging beam, with attenuation length 15 gm/cm^2, and a plane atmosphere are assumed.

Thus, in each case we find $\Phi(\lambda',0) \sim R/\ell$, where R is the range of an average primary, and $\Phi(\lambda', \pi/2) \approx 1$.

The functions $\Psi(\lambda',\phi)$ obtained from the above models are shown in Figure 2. In each case it is assumed that $\Psi(\lambda',\phi)$ vanishes for $\lambda' < \lambda_c$ and is independent of λ' for $\lambda' > \lambda_c$. This is a good approximation, since the latitude interval over which the cutoff energy varies from 10 to 100 Mev is

quite narrow (the Störmer cutoff is 10 Mev at $\lambda' = 72$ degrees and is 100 Mev at $\lambda' = 66$ degrees, assuming vertical incidence) and the contribution from primaries with energies above 100 Mev is assumed to be negligible. However, cutoff rigidities are often reduced during cosmic ray increases. Cosmic rays with energies as low as 120 Mev have, at times of magnetic activity, been observed at Minneapolis (Reference 20). The geomagnetic latitude of Minneapolis, defined so that the vertical cutoff is $14.9 \cos^4 \lambda'$ Bv, is 57.4 degrees (Reference 21) at quiet times although protons of this energy should normally be excluded below about 65 degrees. We therefore carry out the calculation for $\lambda_c = 60$ and 55 degrees.

INJECTION COEFFICIENTS

The basic principle determining the rate of injection into a given orbit is that injection occurs only over those segments of the orbit in which the orbit points toward the source (Reference 9). The decay proton maintains the direction of flight of the parent neutron. As the orbit spirals through space, the velocity vector of a particle in that orbit sweeps out a cone called the α-cone, where α is the local pitch angle. Over some parts of the orbit, the α-cone may miss the earth entirely. The intersection of the α-cone with the earth is called the α-trace. (Only a fraction of the α-trace may fall within the polar cap.) The albedo intensity varies from point to point along the α-trace depending on the zenith angle ϕ made by the velocity vector, and the magnetic latitude λ' of the point of intersection with the earth. Thus, ϕ and λ' may be regarded as "α-trace coordinates."

Since particles are trapped for times that are long compared to bounce periods, it is sufficient to calculate the average injection rate over the orbit. We label an orbit by its coordinates in the equivalent dipole coordinate system discussed by McIlwain (Reference 22). Thus, an orbit is determined by $L = r_o/r_e$, where r_e is the earth's radius, and by the equatorial pitch angle α_o.

At a given point along the orbit, the position of the velocity vector relative to the meridian plane is denoted by θ, the phase angle. The local injection rate at latitude λ, energy E, and phase angle θ is then

$$q(E,L,\alpha_o;\ \lambda,\theta) = \frac{j_n(E,\lambda',\phi)}{t_n v} , \tag{14}$$

where λ' and ϕ are functions of L, α_o, λ and θ. In Equation 14, t_n is the mean lifetime of the neutron (including relativistic time dilation) and v is the neutron's velocity. Assuming that a negligible number of neutrons decay enroute, no correction is necessary for the distance from the earth. That is, since j_n is the differential unidirectional intensity, its value at the point of decay equals its value at the earth.

The quantity q must now be integrated over the spiral path. (The length of the spiral path may be expressed in terms of the distance r_o as $s(\alpha_o)r_o$ where $s(\alpha_o)$ is dimensionless.)

Since the gyrofrequency is large compared to the bounce frequency $v/4s(\alpha_o)\ r_o$, we may average over the phase angle (i.e., over a gyroperiod) before integrating over $s(\alpha_o)$. Thus, the average injection rate $\bar{q}(E,L,\alpha_o)$ is

$$\bar{q}(E,L,\alpha_o) = \frac{1}{s(\alpha_o)} \int_o^{\lambda_m} \langle q(E,L,\lambda) \rangle \frac{ds}{d\lambda} d\lambda , \tag{15}$$

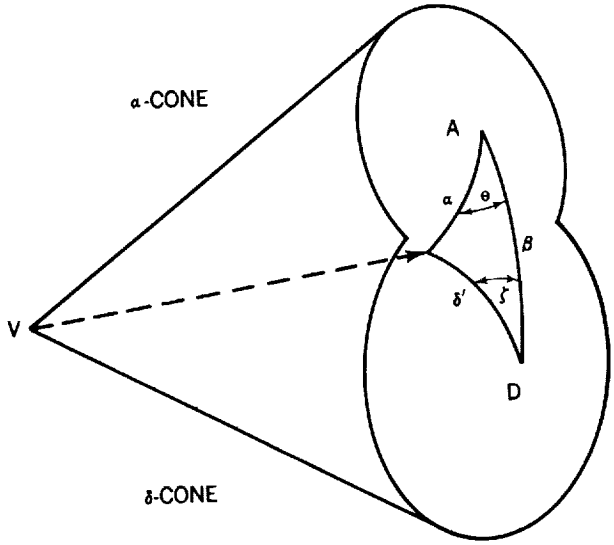

Figure 3a - Two cones are constructed, each with its vertex at V, the guiding center. The α-cone is swept out by the gyrating velocity vector. The δ-cone is the cone subtended by the earth. The point A marks the axis of the α-cone; D marks the axis of the δ-cone. The angle between the two axes is β. When the two cones overlap, the end of the velocity vector, shown as a dashed line, traces out an arc within the δ-cone which we call the α-trace (not shown). The arc AD is a segment of the meridian. The angle θ is the phase angle; as θ varies, the angles δ' and ζ also vary but α and β remain fixed.

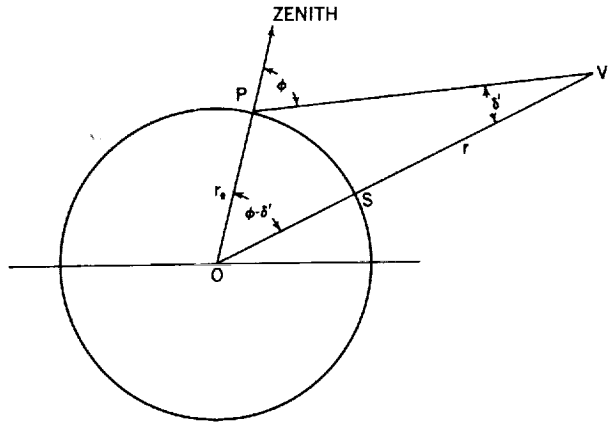

Figure 3b - The circle represents the earth. The line VP is the velocity vector. The point S is the intersection of the axis of the δ-cone with the earth's surface.

where

$$\langle q(E,L,\lambda) \rangle = \frac{1}{2\pi} \int_o^{2\pi} q(E,L,\lambda,\theta)\, d\theta \tag{16}$$

is the average over a gyroperiod, holding λ fixed. We denote the mirror point latitude by λ_m.

We now use Equation 6 to express $\bar{q}$ in terms of j_n^*:

$$\bar{q}(E,L,\alpha_o) = \frac{\epsilon(L,\alpha_o)\, j_n^*(E)}{t_n v} , \tag{17}$$

where the injection coefficient $\epsilon(L,\alpha_o)$ is

$$\epsilon(L,\alpha_o) = \frac{1}{s(\alpha_o)} \int_o^{\lambda_m} \Omega(L,\alpha_o,\lambda) \frac{ds}{d\lambda} d\lambda \tag{18}$$

and

$$\Omega(L,\alpha_o,\lambda) = \frac{1}{\pi} \int_o^{\pi} \Psi(L,\alpha_o,\lambda,\theta)\, d\theta . \tag{19}$$

where $\Psi(L,\alpha_o,\lambda,\theta)$ is the albedo angular distribution function defined by Equation 6, now expressed in orbit coordinates L, α_o, λ, and θ.

Our task now is to relate the orbit coordinates L, α_o, λ, and θ to the α-trace coordinates ϕ and λ'.

For a given orbit, defined by L and α_o, and for some point along the line of force, defined by the latitude λ, we may construct the α-cone and examine its intersection with the earth (see Figure 3). If λ is held fixed and the phase angle θ is varied, the velocity vector will trace out the α-trace on the earth's surface. The latitude λ' at which the vector intersects the earth is given by

$$\lambda' = \lambda + \lambda_1 , \tag{20}$$

where $\lambda_1 = \lambda_1(\theta,\lambda,L,\alpha_o)$. The zenith angle ϕ at this point is related to the orbit coordinates by

$$\sin\phi = L\cos^2\lambda \sin\delta', \tag{21}$$

where

$$\cos\delta' = \cos\alpha\cos\beta + \sin\alpha\sin\beta\cos\theta, \tag{22}$$

$$\sin\alpha = \frac{\left(4 - 3\cos^2\lambda\right)^{1/4}\sin\alpha}{\cos^3\lambda}, \tag{23}$$

and

$$\tan\beta = \frac{1}{2}\cot\lambda. \tag{24}$$

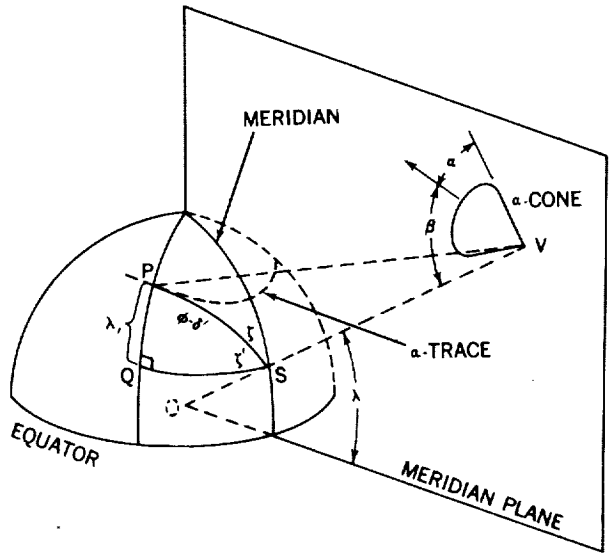

Figure 3c - The axis of the δ-cone passes through the point S. The arc SQ is drawn along a line of constant latitude. The triangle of Figure 3b lies in a plane containing the points P, S, and O, the center of the earth.

Having determined ϕ and δ' from Equations 21 through 24, we may then find λ_1 from

$$\sin\lambda_1 = \cos\zeta \sin(\phi - \delta'), \tag{25}$$

where

$$\cos\zeta = \frac{\cos\alpha - \cos\delta'\cos\beta}{\sin\delta'\sin\beta}. \tag{26}$$

With these relations we are able to compute ϕ and λ' everywhere along the α-trace; thus, Ω can now be evaluated from Equation 19. The integration of Equation 18 is then carried out with the aid of the relation

$$\frac{ds}{d\lambda} = \left(4 - 3\cos^2\lambda\right)^{1/2}\sec\alpha\cos\lambda. \tag{27}$$

The mirror point latitude is related to α_e by

$$\sin\alpha_e = \frac{\cos^3\lambda_m}{\left(4 - 3\cos^2\lambda_m\right)^{1/4}}, \tag{28}$$

and a close approximation to $s(\alpha_o)$ is given by Reference 23

$$s(\alpha_o) \approx 1.38 - 0.32\left(\sin\alpha_o + \sin^{1/2}\alpha_o\right). \tag{29}$$

When the α-cone does not intersect the earth, Ω is zero. For an orbit such that $\Omega(L,\alpha_o,\lambda) = 0$ for $\lambda = 0$, the latitude λ_2 such that the α-cone first touches the earth may be obtained from the implicit relation

$$\alpha(\lambda_2) + \delta(\lambda_2) = \beta(\lambda_2) , \tag{30}$$

where

$$\sin \delta = \frac{\sec^2\lambda}{L} . \tag{31}$$

The angle δ is the semiangle of the cone drawn from the orbit point to the earth, the cone being tangent to the earth's surface.

In general, only a part of the α-cone intersects the earth. In this case, the upper limit on the integral in Equation 19 is replaced by θ', where

$$\cos\theta' = \frac{\cos\delta - \cos\alpha\cos\beta}{\sin\alpha\sin\beta} . \tag{32}$$

The angle θ' is related to the injection coefficient $\overline{\eta}_o$ calculated by Singer (Reference 9) through

$$\overline{\eta}_o = \frac{1}{s(\alpha_o)} \int_o^{\lambda_m} \eta(\lambda) \frac{ds}{d\lambda} d\lambda \tag{33}$$

and

$$\eta(\lambda) = \frac{\theta'}{\pi} . \tag{34}$$

If we assume an isotropic albedo and intensity uniform with respect to latitude, then ϵ reduces to $\overline{\eta}_o$.

The injection coefficients have been evaluated for the orbits which mirror at the points in space where the NERV observations were made. The coordinates of these points are given in Table 1 along with the coefficients calculated from the albedo distribution of Model 3. The most important feature

Table 1
Injection Coefficients for Orbits Mirroring at the Locations of the NERV Observations

L = equivalent geocentric distance in equatorial plane; α_o = equatorial pitch angle; λ_2 = latitude of particle when the α-cone first intersects the earth; $\lambda^\dagger$ = highest latitude on earth's surface attained by the α-trace; ϵ_{60} = injection coefficient assuming solar cosmic rays reach latitude 60 degrees; ϵ_{55} = injection coefficient assuming solar cosmic rays reach latitude 55 degrees.

Point Number	L	cos α_o	λ_2	$\lambda^\dagger$	ϵ_{60}	ϵ_{55}
3	1.79	0.866	11.0	66.1	0.15	0.29
4	1.72	0.832	9.0	62.3	0.10	0.18
5	1.54	0.775	5.5	54.5	0	0
6	1.47	0.755	2.9	48.3	0	0

Table 2
Minimum Injection Distance L_{min} as a Function of the Latitudes of the Boundary of the Polar Cap λ_c (Assuming Infinite Atmospheric Density Below 1270 km).

λ_c (degrees)	L_{min} (earth radii)
0	1.20
10	1.22
20	1.27
30	1.32
40	1.38
50	1.46
60	1.65
70	1.88
80	2.30

of the result is that the injection coefficient is zero at points 5 and 6. These are the points at which the anomalous component is absent. It can be shown that for a given value of λ_c there is a minimum value of L for which any injection is possible (for any value of α_o). In Table 2 we give L_{min} as a function of λ_c. Note that for $\lambda_c \approx 60$ degrees, the boundary of the accessible region is at L = 1.65; this is consistent with the observations.

The vanishing of the injection coefficient at the two inner points argues against an interpretation of the anomalous component in terms of either direct injection from the solar plasma cloud or local acceleration. Both of these mechanisms seem unlikely to produce trapped radiation with such a sharp lower boundary. The polar albedo mechanism, however, leads to a sharp lower boundary in just the correct range of L.

The reason for the absence of injection at the inner points may be more clearly seen by considering the behavior of the α-cone or the α-trace as λ varies. All four orbits are of the class in which the α-cone does not intersect the earth when the vertex of the cone is at the equatorial plane. As λ increases, the α-cone tilts toward the earth and grows wider. When the vertex reaches λ_2 the α-cone is just tangent to the earth.

As λ is further increased, the α-trace moves across the globe in a generally equatorward direction. The maximum latitude $\lambda^\dagger$ attained by any part of the α-trace is given in Table 1. We see that for the first two orbits $\lambda^\dagger$ is greater than 60 degrees. However, the α-traces of points 5 and 6 never get within the source region, which is assumed to be confined to latitudes $> \lambda_c = 60$ degrees. With this value of λ_c the α-trace for point 3 first enters the source region when $\lambda = 11.0$ degrees and leaves the source region when $\lambda = 13.4$ degrees. Thus, injection takes place only over a very small part of the total orbit (which mirrors at 32.2 degrees). The corresponding range for point 4 is 9.0 degrees to 9.7 degrees.

In comparing ϵ with the corresponding coefficients $\bar{\eta}_o$ calculated for the global component (Reference 9) it should be noted that the latter coefficient refers to an isotropic albedo whose strength is independent of latitude.

INTENSITY OF THE ANOMALOUS COMPONENT

Using the values $\sigma_o = 80$ mb, $\ell = 15$ gm/cm^2, and $\Phi^* = 0.025$ (Model 3) we obtain

$$j(E,L,\alpha_o) = 6.4 \times 10^{-4}\, \epsilon(L,\alpha_o)\, S(E)\, J_o \frac{t_o}{t_n} \tag{35}$$

for the differential, directional intensity of newly trapped protons following an injection "impulse" of duration t_o. For the NERV points (ϵ on the order of 0.1) we therefore have an integral directional intensity J(E) above 10 Mev on the order of $1.8 \times 10^{-8}\, J_o t_o$ p/cm^2-ster-sec.

Now, the intensities observed at the NERV points (3 and 4) were approximately 10^3 p/cm^2-ster-sec. In order to account for these intensities on the basis of impulsive injection from a single event we require $J_o t_o$ to be approximately 5×10^{10}. The September 3, 1960, event (16 days prior to the date of the observations) was therefore far too small.

The events of July, 1959, contributed a time-integrated flux $J_o t_o$ of approximately 5×10^8 while the large storm of February, 1956, reached approximately 10^9 p/cm^2-ster. However, to evaluate the contribution from these less recent events we need to consider the lifetimes of the protons.

If protons are adiabatically trapped, then their lifetime, as determined by energy loss, is inversely proportional to the exospheric density averaged over the orbit. Assuming a hydrogen exosphere, 50 percent ionized, the 1/e lifetime, defined as the time over which the energy decreases to 1/e times the initial value, is given by

$$T_{1/e} = 10^{11} \frac{E^{1.5}}{\bar{\rho}} \text{ seconds}, \tag{36}$$

where E is the initial energy in Mev and $\bar{\rho}$ is the average density (atoms-and-ions/cm^3). This expression is valid for E < 300 Mev. For orbits that mirror above approximately 1500 km $\bar{\rho}$ is less than 10^4/cm^3. Therefore, if 10 Mev protons are adiabatically trapped their lifetime is 10 years or more.

The length of this lifetime suggests the possibility that an equilibrium exists, with injection from large events at irregular intervals of a few years being averaged over several events. Webber (Reference 21) has collected data on some twenty solar cosmic ray events since 1956. For most of these events the intensity only above about 100 Mev is known. We have extrapolated each spectrum to 10 Mev by assuming a spectrum J_o proportional to $T^{-1.3}$ below 100 Mev (see Table 3).

Table 3
Time-Integrated Solar Cosmic Ray Intensities Above 10 Mev.*

Date	$\frac{J_o t_o}{\text{particles}/\text{cm}^2\text{-ster}} \times 10^{-6}$	Reference
February 23, 1956	1000	21
July 7, 1958	10	21
August 22, 1958	4	21
May 11, 1958	7	21
July 10, 1959	8	21
July 14, 1959	140	21
July 17, 1959	400	21
April 1-2, 1960	2	24
April 28-30, 1960	1	24
April 4-7, 1960	1	24
September 3, 1960	0.6	18
September 3-9, 1960	0.8	24
November 12-14, 1960	640	24
November 15, 1960	180	24
November 12-15, 1960	1000	19
November 20-26, 1960	20	24

*In each case extrapolations down to 10 Mev have been made assuming J_o proportional to $T^{-1.3}$ except for the September and November, 1960, events where spectra directly observed in References 18 and 19 were used.

We find that over a period of about 5 years prior to the November 1960 events solar cosmic rays contributed a total of approximately 1.5×10^9 particles/cm^2-ster over the polar caps. This represents an average rate $\bar{J}$ of about 10 particles/cm^2-ster-sec, about 100 times the galactic rate.

An estimate of the equilibrium intensity from "continuous" polar injection is obtained by replacing $J_o t_o$ in Equation 35 by $\bar{J} T_{1/e}$. Thus, this process can account for the observations provided $\bar{\rho} \approx 10^3/\text{cm}^3$.

We therefore suggest that the "anomalous" component is a permanent feature. It might be called the polar component.

Since the injection is intermittent the polar component will behave as an equilibrium distribution only at energies that are high enough to make the lifetimes long compared to the interval between injection events. The lower end of this energy range will vary with altitude, i.e., with exospheric density, approximately as $r^{-2\nu/3}$ in a region where the density varies as $r^{-\nu}$.

In more detail, the equilibrium spectrum is found by integrating the continuity equation

$$\bar{q} = \frac{\partial}{\partial E}\left[n \frac{\partial E}{\partial t}\right], \tag{37}$$

assuming that v is proportional to $E^{1/2}$ and

$$\frac{\partial E}{\partial t} = -k\bar{\rho}E^{-1/2}, \tag{38}$$

where $k = 7.65 \times 10^{-12}$ Mev$^{3/2}$-cm^3/sec for E in Mev. We find

$$j = \frac{\sigma_o \ell \Phi^* \Theta^{1/2}}{2\sqrt{\pi} k t_n} \frac{\epsilon \bar{J}}{\bar{\rho}} F = 1.7 \times 10^5 \frac{\epsilon \bar{J} F}{\bar{\rho}}, \tag{39}$$

where $\epsilon = \epsilon(E, \alpha_o)$ and

$$F = F(E/\Theta) = \frac{E}{\Theta} \int_{E/\Theta}^{\infty} e^{-y} y^{1/2} dy. \tag{40}$$

The function F is related to functions tabulated by Pearson (Reference 25) and is shown in Figure 4.

Before a comparison with the observations can be made we must take into account that, on the hypothesis of this paper, the spectrum at points 3 and 4 represents a superposition of a

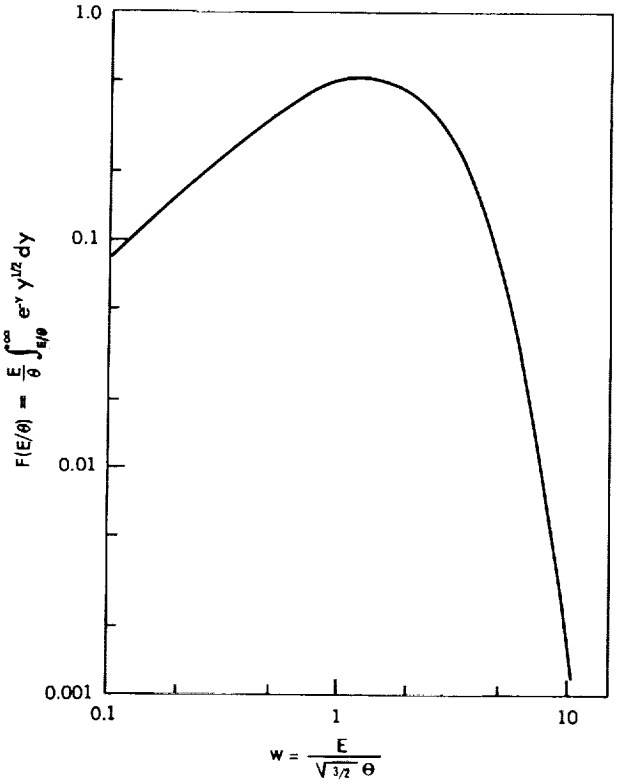

Figure 4 - The equilibrium energy spectrum resulting from injection with the Maxwellian spectrum and slowing down by pure energy loss is proportional to F(w), where $E = \sqrt{3/2}\ \Theta w$.

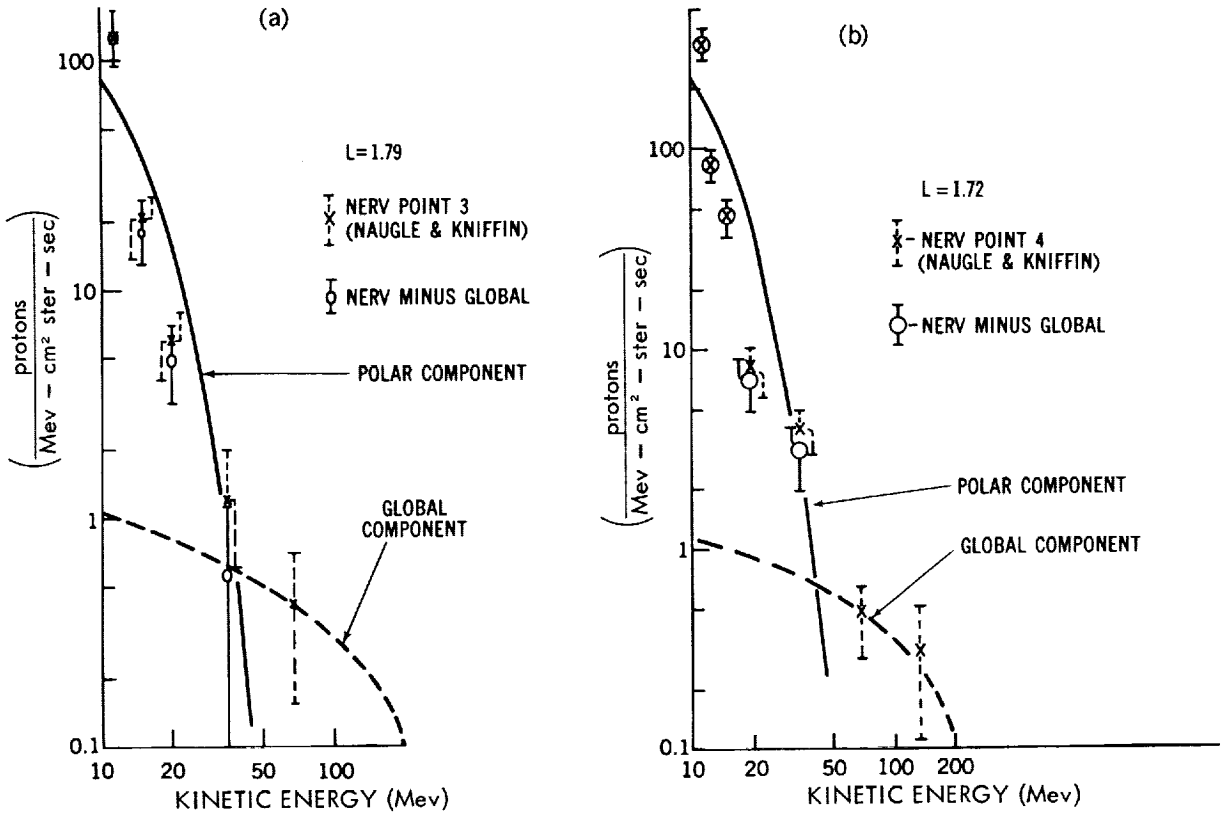

Figure 5 - Comparison between equilibrium spectrum and observations. The "global component" represents the spectrum observed at the innermost point, normalized to the data at 20 Mev. This component is subtracted from the observations (crosses) to give the anomalous component (circles). The heavy solid curve is the computed spectrum, normalized by the choice of density $\bar{\rho}$. In 5a, L = 1.79, $\bar{\rho} = 1.06 \times 10^3/cm^3$ and in 5(b), L = 1.72, $\bar{\rho} = 2.6 \times 10^2/cm^3$. These intensities are computed with an assumed average solar cosmic ray flux $\bar{J} = 10$ particles/cm²-ster-sec > 10 Mev.

polar component upon the global component. We therefore take the spectrum seen at points 5 and 6, normalized to the data at 70 Mev, to be the global component and subtract this intensity from the anomalous spectrum.

The result for point 3 is shown in Figure 5A along with the spectrum computed from Equation 39 and normalized by setting $\bar{\rho}_3 = 1.06 \times 10^3/cm^3$. The corresponding result for point 4, using $\bar{\rho}_4 = 260/cm^3$, is shown in Figure 5B. Noting that the neutron spectrum is only approximately given by the Maxwellian which we have assumed and that we have neglected the modulation of the albedo spectrum which will result from energy degradation in the atmosphere we regard the agreement as at least fair. (The latter effect will tend to steepen the spectrum at the low energy end and to fill in the region below the peak in the source spectrum.)

An important point should be noted. The relative intensities at points 3 and 4 are about 1:3. That is, the higher intensity is found on the inner shell (L = 1.72). Now the intensity ratio is predicted to be $\epsilon_3 \bar{\rho}_4 / \epsilon_4 \bar{\rho}_3$, using subscripts to denote the number of the point. Since $\epsilon_3/\epsilon_4 \approx 1.5$ we require $\bar{\rho}_3/\bar{\rho}_4 \approx 4$. The average densities are proportional to the mirror point densities. Orbit 3 mirrors at 1600 km and orbit 4 mirrors at 1884 km. If the temperature is approximately 2000°K at the base of

the exosphere then these mirror points will fall within the region in which oxygen predominates over hydrogen. The scale height of exospheric atomic oxygen at 1600 km is about 164 km for T = 2000 °K, leading to a ratio of mirror point densities exp [(1884-1600)/164] = 5.6. (If O^+ contributes strongly then this ratio will be reduced. A pure O^+ atmosphere leads to a ratio exp [284/(2x164)] = 2.4.) We conclude therefore that the relative intensities at the NERV points 3 and 4 are consistent with our knowledge of the exosphere and do not indicate a breakdown of the trapping condition at these low energies (below 30 Mev).

SPATIAL DISTRIBUTION

The spatial distribution produced by this mechanism is characterized by two prominent features: (1) a *shadow zone* is formed close to the earth within which no "polar protons" are trapped, (2) beyond the shadow zone trapping is possible. However, there is a range of equatorial pitch angles

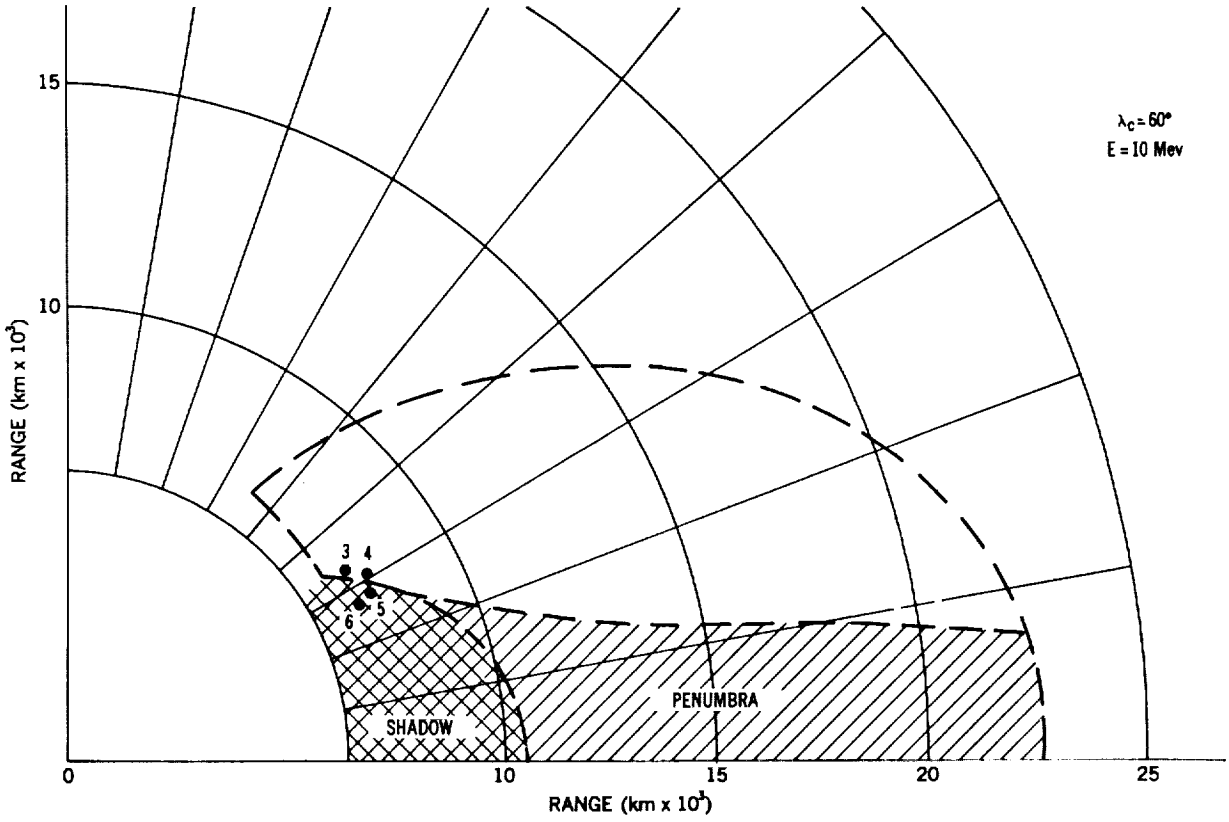

Figure 6 - Shadow zone and penumbra formed by polar cap injection. There is no trapping of fast protons at all in the shadow zone. Polar protons are trapped in the penumbra but they do not mirror in this region. The unshaded area may contain polar protons at all local pitch angles outside of the loss cone. The outer boundary of this region depends on energy as there is a maximum energy of proton which may remain trapped at a given L. The boundary drawn here corresponds to 10-Mev protons, assuming $E_{max} = 1600\,L^{-4}$ Mev (Reference 26). The points labeled 3, 4, 5, 6 are the locations of the NERV observations (Reference 1).

centered about 90 degrees within which no injection takes place. This leads to the existence of a *penumbra*, a region in which the polar component is present at local pitch angles less than 90 degrees but does not mirror.

The shadow zone and penumbra formed by a polar cap source with boundary at $\lambda_c = 60$ degrees are shown in Figure 6. The shape of the penumbra is not a strong function of λ_c. Its boundary remains approximately parallel to the equatorial plane as λ_c is varied from about 30 to 90 degrees. The boundary of the shadow zone is always a magnetic shell of course.

PROTONS IN THE OUTER BELT

The polar mechanism injects about 100 times more low energy protons per Mev at about 10 Mev into the outer belt than does the global source. However, it is believed that the trapping ability of the quiescent field decreases at great altitudes. A variation of maximum trappable energy with altitude of the form E_{max} = constant $\times L^{-4}$ has been predicted by Singer (Reference 26). Normalization of this relation is provided by satellite observations of the radial extent of 75-Mev protons (Reference 27), leading to $E_{max} = 1600\, L^{-4}$ Mev. On this model, 1-Mev protons may remain trapped up to $L = 6.3$, 10-Mev protons up to $L = 3.6$, etc.

We may therefore expect to find the "polar" low-energy component extending to the heart of the outer zone or beyond. The intensity at a given energy should increase with altitude (as both ϵ and $1/\overline{\rho}$ increase) until E exceeds $E_{max}(L)$.

CONCLUSION

We have shown that the lower boundary of the proton belt produced by solar cosmic rays through the intermediary of albedo neutrons is consistent with the observed spatial distribution of low-energy protons in the inner zone. The energy spectrum of the high-latitude component is approximately accounted for (above 10 Mev) assuming secondary neutrons are generated in an evaporation spectrum and that the decay protons are in equilibrium. The absolute intensities roughly agree with experiment, assuming a reasonable source strength and atmospheric model.

In addition to the more obvious experimental tests such as extending the observations to lower energies and to higher L-values and such as repeating the same observations at a later time to look for time variations, we may point out that the polar source leads to a peculiar angular distribution (equatorial orbits are not populated) which can be investigated observationally (Lenchek and Singer, 1962).

ACKNOWLEDGMENTS

The author sincerely appreciates the close cooperation of J. Naugle and D. Kniffen. A part of this work has been submitted in partial fulfillment of the requirements for the PhD degree at the University of Maryland, thesis research under the direction of Prof. S. F. Singer and partially supported

by a fellowship awarded by the National Rocket Club, Washington, D. C. The author is grateful to the National Aeronautics and Space Administration and the University of Maryland for their cooperation in this regard. Also, he acknowledges very helpful discussions with C. E. Fichtel and C. J. Waddington.

REFERENCES

1. Naugle, J. E., and Kniffen, D. A., "Flux and Energy Spectra of the Protons in the Inner Van Allen Belt," *Phys. Rev. Letters* 7 (1):3-6, July 1, 1961

2. Freden, S. C., and White, R. S., "Particle Fluxes in the Inner Radiation Belt," *J. Geophys. Res.* 65 (5):1377-1383, May 1960

3. Lenchek, A. M., and Singer, S. F., "Geomagnetically Trapped Protons from Cosmic-Ray Albedo Neutrons," *J. Geophys. Res.* 67 (4):1263-1287, April 1962

4. Singer, S. F., "Trapped Albedo Theory of the Radiation Belt," *Phys. Rev. Letters* 1 (5):181-183, September 1, 1958

5. Vernov, S. N., Grigorov, N. L., et al., "Possible Mechanism of Production of 'Terrestrial Corpuscular Radiation' Under the Action of Cosmic Rays," *Doklady Akademii Nauk SSSR* 124 (5): 1022-1025, February 11, 1959 (In Russian); Translation in *Soviet Phys.-Doklady* 4 (1):154-157, August 1959

6. Armstrong, A. H., Harrison, F. B., et al., "Charged Particles in the Inner Van Allen Radiation Belt," *J. Geophys. Res.* 66 (2):351-357, February 1961

7. Lenchek, A. M., and Singer, S. F., "Injection of Trapped Protons from Solar Flare Particles," in: *Proc. Internat. Conf. on Cosmic Rays and the Earth Storm, Kyoto, September 1961. II. Joint Sessions*, Tokyo: Physical Society of Japan, 1962, pp. 123-127

8. Wentworth, R. C., and Singer, S. F., "The Albedo Contribution in the Measurement of Cosmic-Ray Primaries," *Phys. Rev.* 98 (5):1546-1547, June 1, 1955 (Abstract)

9. Singer, S. F., "Latitude and Altitude Distribution of Geomagnetically Trapped Protons," *Phys. Rev. Letters* 5 (7):300-303, October 1, 1960

10. Kellogg, P. J., "Electrons of the Van Allen Radiation," *J. Geophys. Res.* 65 (9):2705-2713, September 1960

11. Hess, W. N., Canfield, E. H., and Lingenfelter, R. E., "Cosmic-Ray Neutron Demography," *J. Geophys. Res.* 66 (3):665-677, March 1961

12. Tai, Y.-K., Millburn, G. P., et al., "Neutron Yields from Thick Targets Bombarded by 18- and 32-Mev Protons," *Phys. Rev.* 109 (6):2086-2091, March 15, 1958

13. Ajzenberg, F., and Franzen, W., "Neutrons from the Proton Bombardment of N^{14}," *Phys. Rev.* 94 (2):409-411, April 15, 1954

14. Adelson, H. E., "Energy Spectra and Angular Dependences of Neutrons from the 31.5-Mev Proton Bombardment of Beryllium-9, Nitrogen-14 and Aluminum-27," Univ. Calif., Lawrence Radiation Lab., UCRL-8568, December 11, 1958

15. Blatt, J. M., and Weisskopf, V. F., "Theoretical Nuclear Physics," New York: John Wiley and Sons, 1952, p. 350, equation (4.5)

16. Le Couteur, K. J., "The Evaporation Theory of Nuclear Disintegrations," *Proc. Phys. Soc. (London)* 63A (3):259-282, March 1950

17. Rossi, B. R., "High-Energy Particles," New York: Prentice-Hall, 1952, p. 344

18. Davis, L. R., Fichtel, C. E., et al., "Rocket Observations of Solar Protons on September 3, 1960," *Phys. Rev. Letters* 6 (9):492-494, May 1, 1961

19. Ogilvie, K. W., Bryant, D. A., and Davis, L. R., "Rocket Observations of Solar Protons during the November 1960 Event," in: *Proc. Internat. Conf. on Cosmic Rays and the Earth Storm, Kyoto, September 1961. II. Joint Sessions,* Tokyo: Physical Society of Japan, 1962, pp. 317-319; also "Rocket Observations of Solar Protons During the November 1960 Events, I," *J. Geophys. Res.* 67 (3):929-937, March 1962

20. Freier, P. S., Ney, E. P., and Winckler, J. R., "Balloon Observation of Solar Cosmic Rays on March 26, 1958," *J. Geophys. Res.* 64 (6):685-688, June 1959

21. Webber, W. R., "Time Variations of Low Energy Cosmic Rays during the Recent Solar Cycle," in: *Progress in Elementary Particle and Cosmic Ray Physics,* ed. by J. G. Wilson and S. A. Wouthuysen, Amsterdam: North-Holland Publ. Co., Vol. 6, 1962 (In Press)

22. McIlwain, C. E., "Coordinates for Mapping the Distribution of Magnetically Trapped Particles," *J. Geophys. Res.* 66 (11):3681-3691, November 1961

23. Wentworth, R. C., "Lifetimes of Geomagnetically Trapped Particles Determined by Coulomb Scattering," Ph.D. Thesis, University of Maryland, 1960

24. Lin, W. C., "Observation of Galactic and Solar Cosmic Rays from October 13, 1959 to February 17, 1961 with Explorer VII (Satellite 1959 Iota)" State Univ. of Iowa SUI-61-16, August 1961 (Thesis submitted for M.S. degree)

25. Pearson, K., "Tables of the Incomplete Gamma-Function," Cambridge: The University Press, 1957 (Reprint of 1922 edition)

26. Singer, S. F., "Cause of the Minimum in the Earth's Radiation Belt," *Phys. Rev. Letters* 3 (4): 188-190, August 15, 1959

27. Fan, C. Y., Meyer, P., and Simpson, J. A., "Dynamics and Structure of the Outer Radiation Belt," *J. Geophys. Res.* 66 (9):2607-2640, September 1961